

## Evaluation of thermoelectric and transport properties in $\text{Fe}_{1-x}\text{Mn}_x\text{VSb}$ half-Heusler system synthesized by mechanical alloying process

Rahidul Hasan and Soon-Chul Ur\*

Department of Materials Science and Engineering/ReSEM, Korea National University of Transportation, 50 Daehak-ro, Chungju, Chungbuk 27469, Republic of Korea

Mechanical alloying followed by subsequent vacuum hot pressing was utilized for the synthesis of  $\text{Fe}_{1-x}\text{Mn}_x\text{VSb}$  ( $0.01 \leq x \leq 0.05$ ) half-Heusler alloys. Controlling doping concentration could make a major effect on thermoelectric properties of this system. Near single half-Heusler phases were found to be dominating in all the samples, however, a fraction of second phases also traced. Investigation of microstructure revealed that ultrafine microstructure was formed in vacuum hot pressed samples. Thermoelectric properties were studied as a function of doping concentration and temperature. The absolute value of Seebeck coefficient was found to be increased with increasing temperature and doping concentration. Electrical conductivity was found to be decreased slightly with increasing temperature. Thermal conductivity and lattice thermal conductivity decreased considerably with increasing temperature, which could be due to increasing effective mass, grain boundary scattering, second phase interaction, and substitutional defect. The resultant maximum thermoelectric figure of merit was found to be 0.21 for  $x = 0.03$  at 567 K. No incorporation of foreign elements was found during handling and processing.

**Key words:** Doping, Seebeck Coefficient, Thermal Conductivity, Half-Heusler

### Introduction

Fossil fuel is the primary source of energy for this universe right now, and the reserves are terminating very quickly. The energy research world is therefore constantly striving to find an alternative sustainable energy source. A research conducted by a research group showed that two-thirds of our total energy is wasted as heat during utilization process [1]. In recent times, researchers are converting waste heat into electrical energy by means of thermoelectric (TE) generator [2]. This process is very effective and beneficial as it doesn't require any moving-mechanical parts. Moreover, the system is noise free and the ingredients used are relatively cheaper. TE efficiency of a material system is directly dependant on its dimensionless figure of merit (ZT), which can be defined as,  $ZT = S^2\sigma T/\kappa$ , where  $S$  = Seebeck coefficient,  $\sigma$  = electrical conductivity,  $T$  = absolute temperature and  $\kappa$  represents thermal conductivity [2].

Half-Heusler (HH) is a new class of TE material that showed some sort of improvement in TE efficiency [3]. The notable TE feature that attracts it as a good TE material is the high Seebeck coefficient of around  $100 \mu\text{VK}^{-1}$  with good thermal and mechanical stability [4]. Most of the reported HH materials showed moderate

temperature dependent ZT value. Among the HH systems,  $\text{MNiSn}$  [4] and  $\text{MCoSb}$  [5] showed high temperature dependent ZT, where  $M = \text{Ti, Zr, and Hf}$ . In recent times,  $\text{FeVSb}$  HH was found to be effective TE material due to its low band gap [6]. The main obstacle of this system is the thermal conductivity of around  $10\sim 13 \text{ Wm}^{-1}\text{K}^{-1}$  [7], which is really high for a practical TE device. Zou et al. reported that thermal conductivity in  $\text{FeVSb}$  HH systems can be reduced to  $4\sim 5 \text{ Wm}^{-1}\text{K}^{-1}$  by boundary scattering process during the formation of ultrafine microstructures [8]. Doping is another effective method to reduce thermal conductivity as well. For example, Sb doping in  $\text{MNiSn}$  [9] and Sn doping in  $\text{MCoSb}$  [10] showed considerable reduction in thermal conductivity. ZT value of HH systems can be increased by applying several processes. Among them, nanostructuring and doping are noticeable. It was reported that nanostructuring improved ZT value up to more than 1.2 in n-type  $\text{MNiSn}_{1-x}\text{Sb}_x$  [11-13] and around  $0.9\sim 1.0$  in p-type  $\text{MCoSb}_{1-x}\text{Sn}_x$  [14, 15], where  $M = \text{Ti, Zr and Hf}$ . Electron donator or acceptor elements have the capability to optimize the carrier concentration, which may increase the Seebeck coefficient [16]. Usually, dopant acts as an alter point between the host system and the reservoir.

In this study,  $\text{Fe}_{1-x}\text{Mn}_x\text{VSb}$  HH materials were fabricated by mechanical alloying (MA) process and subsequent vacuum hot pressing (VHP). MA process is used because it is a well-known high energy milling technique that can produce ultrafine microstructures [17]. The vacuum hot pressing (VHP) is frequently

\*Corresponding author:  
Tel : +82-43-841-5385  
Fax: +82-43-841-5380  
E-mail: scur@ut.ac.kr

utilized to consolidate the mechanically alloyed powders [17, 18]. The plastic deformation during vacuum hot pressing might introduce diffusion path, leading to relatively easier alloy formation [18]. Thermoelectric and transport properties were evaluated as a function of doping materials and temperature within the range of 300–973 K.

## Experiments

$\text{Fe}_{1-x}\text{Mn}_x\text{VSb}$  ( $0.01 \leq x \leq 0.05$ ) HH alloys were fabricated from the elemental powder (purity ~99.9%) mixtures of Fe (63  $\mu\text{m}$ ), V (75  $\mu\text{m}$ ), Mn (56  $\mu\text{m}$ ) and Sb (45  $\mu\text{m}$ ). MA process was run using a high energy vibrator mill (KMTech TMM-70, Korea) for 8 h with constant speed at 1080 rpm. Small zirconia balls (precisely ~5 mm diameter) were used for the progress of milling (ball-to-powder mixture ratio ~10:1). Consolidation of the MAed powders was done in VHP using a graphite die maintaining at 1073 K temperature and 80 MPa pressure.

Horriba LA-950 (Japan) PSA was used to measure the particle size of the MAed powder. Bruker AXS Advance D-8 (Germany), XRD instrument was utilized to investigate the phase transformation of as-MAed and VHPed samples. FEI Quanta-400 (Netherlands) scanning electron microscopy (SEM) was employed to study the microstructure of VHPed samples. The Seebeck

coefficient and electrical resistivity were measured by 4-probe method using ZEM3 (Japan) instrument.  $3 \times 3 \times 10 \text{ mm}^3$  and  $10 \Phi \times 1 \text{ mm}$  samples were used for the Seebeck coefficient-electrical resistivity and thermal diffusivity measurement, respectively. Thermal diffusivity was measured by laser flash method using TC-9000H (Japan) instrument. Thermal conductivity was calculated using the equation,  $\kappa = \rho \times C_p \times D$ , where  $\rho$  is the density,  $C_p$  is the heat capacity, and  $D$  is the thermal diffusivity. Samples density was calculated by the Archimedes method. Van der Pauw method has been used to measure room temperature Hall coefficient, carrier concentration and carrier mobility.

## Results and Discussion

Round shaped particles are seen from the scanning electron microscope (SEM) images of as-MAed powder. The average particle sizes are found to be less than 10  $\mu\text{m}$ , which is shown in Fig. 1. The average particle size increases with increasing doping concentration and the approximate size were found to be 8.2  $\mu\text{m}$ , 8.3  $\mu\text{m}$ , 9.2  $\mu\text{m}$ , 9.6  $\mu\text{m}$  and 9.8  $\mu\text{m}$ , respectively, for  $x=0.01\sim 0.05$ .

The lattice parameter seems to be increased with increasing dopants concentration (Fig. 2a). It could be due to substitution of smaller Fe (atomic radius 1.26 Å) by larger Mn (atomic radius 1.37 Å) atom [8]. This statement agrees with the Denton *et al.*, which implies

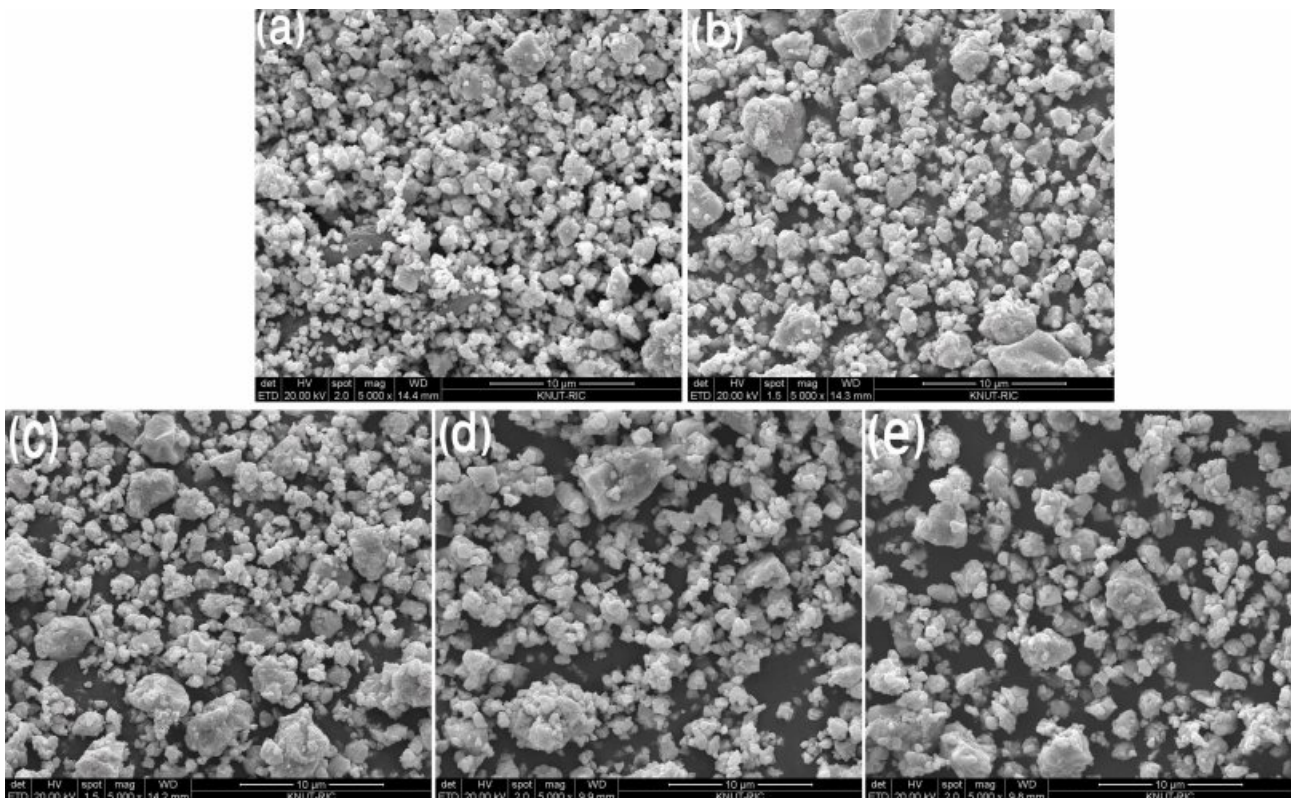


**Fig. 1.** Calculated average particle size of as-MAed powders for 8 h; (a)  $x=0.01$ , (b)  $x=0.02$ , (c)  $x=0.03$ , (d)  $x=0.04$ , and (e)  $x=0.05$ .

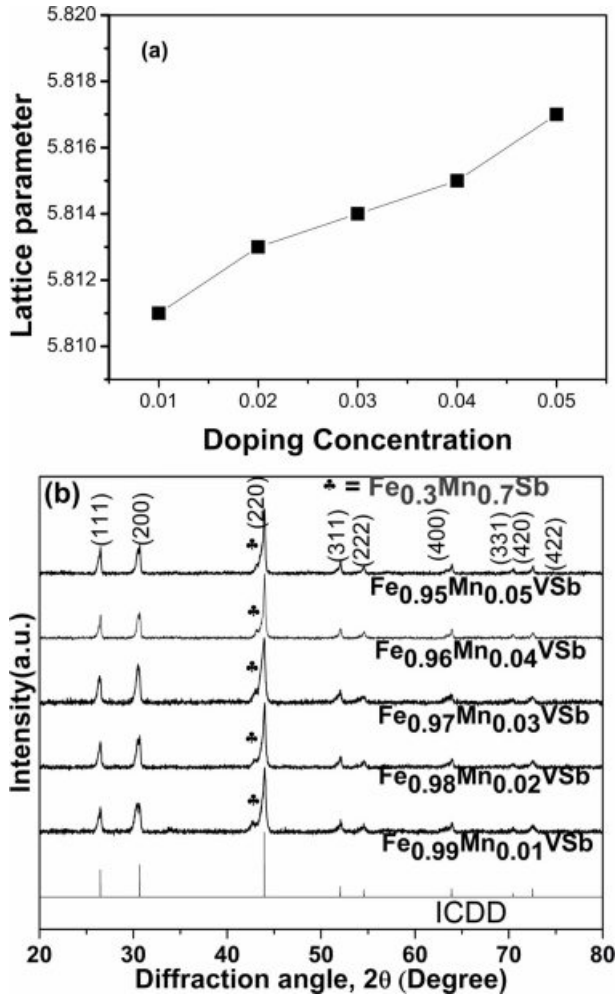


Fig. 2. Change in crystal structure of VHPed samples; (a) lattice parameter as a function of doping concentration, and (b) peak shifting for  $Fe_{1-x}Mn_xVSb$  ( $x=0.01\sim 0.05$ ).

that lattice parameter will be changed with respect to the atomic radius of the doping elements [19]. This increasing lattice parameter could shift the diffraction peak to the smaller diffraction angle (Fig. 2b).

XRD patterns of the as-MAed powders and VHPed samples are shown in Fig. 3. The HH phase formation started from 4h of milling and continued with the milling time. Besides the HH phase, a second phase was also formed in as-MAed powders, which was detected as  $Fe_{0.3}Mn_{0.7}Sb$ . This second phase doesn't completely disappear after VHP, which is clearly shown in Fig. 3(b).

SEM images show that ultrafine microstructure might have formed in all the samples after VHP, as can be seen from the Fig. 4. There is considerable grain growth observed in SEM images which might be influenced by high relative density of VHPed samples. Around 98% relative densities were achieved after VHP which was confirmed by Archimedes method (Fig. 5). SEM was utilized to calculate the grain size and the result showed that the average grain size were

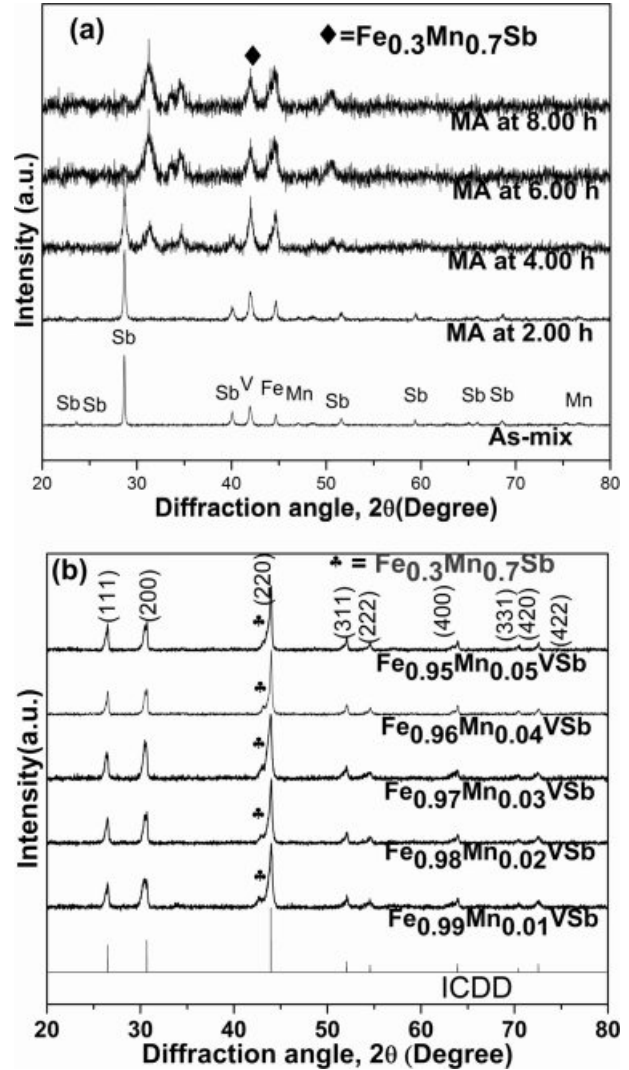
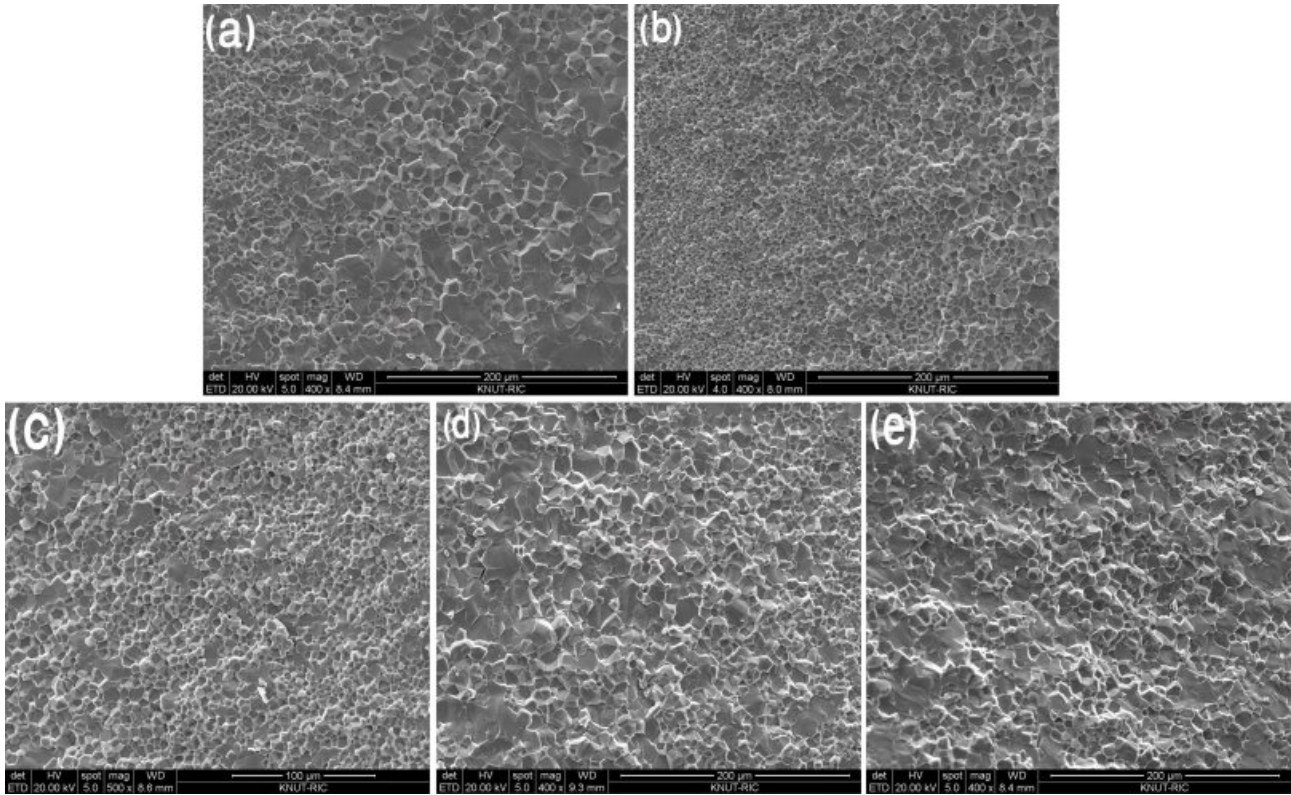


Fig. 3. Phase transition in; (a) MAed powder samples, and (b) near single HH phase with a fraction of secondary phase in VHPed samples.

in the range of 8~10  $\mu m$ .

Fig. 6(a) shows the measured Seebeck coefficient in the temperature range of 300~973 K. The Seebeck coefficient of  $Fe_{1-x}Mn_xVSb$  was found to be very sensitive to the Fe and Mn concentration [20] and the highest sensitivity is found for  $x = 0.02$  sample. The absolute value of the Seebeck coefficient is significantly improved for  $Fe_{0.98}Mn_{0.02}VSb$  at high temperatures possibly due to phonon drag effect [21]. At room temperature, the absolute Seebeck coefficient is found to be in the range of 63~68  $\mu VK^{-1}$  for all the samples. As the temperature rises, the Seebeck coefficient increased for all the samples and a highest value of  $\sim 100 \mu VK^{-1}$  was achieved for  $x = 0.02$ , which was  $\sim 58\%$  improvement from the room temperature. Another cause this increase of seebeck coefficient might be due to the intrinsic transition of electron during high temperature [9]. Carrier concentration



**Fig. 4.** SEM images, which showed the microstructure of VHPed  $\text{Fe}_{1-x}\text{Mn}_x\text{VSb}$ ; (a)  $x=0.01$ , (b)  $x=0.02$ , (c)  $x=0.03$ , (d)  $x=0.04$ , and (e)  $x=0.05$ .

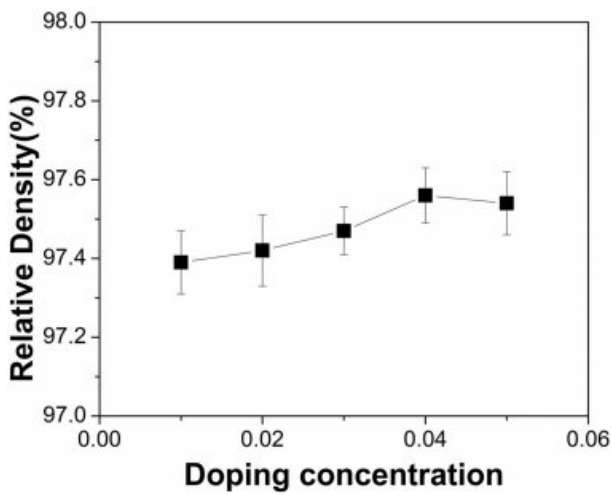


**Fig. 5.** Calculated relative density, as a function of doping concentration.

seems to be slightly decreased with increasing doping elements up to  $x=0.01\sim 0.03$ , as can be seen from Table 2. The effective mass of the carrier and carrier concentration has the strong relationship with the Seebeck coefficient, which can be written as,  $S \propto m^*/n^{2/3}$ , where  $m^*$  is the effective mass of the carriers and  $n$  is the carrier concentration. This equation clearly implies that increasing effective mass has a strong

influence to the increase of Seebeck coefficient.

Temperature dependence of electrical conductivity of  $\text{Fe}_{1-x}\text{Mn}_x\text{VSb}$  is shown by the Fig. 6(b). It can be seen from the figure that electrical conductivity is increased for  $x=0.01\sim 0.03$  but decreased for  $x=0.04\sim 0.05$  at room temperature with increasing Mn concentration and the maximum electrical conductivity is shown by  $x=0.03$  sample. Electrical conductivity decreased gradually by all the samples at elevated temperature, which indicate non-degenerate metallic behavior. Possibly, at high temperature, the grain boundaries might trap some electrons, leading to increase of holes by energy filtering effect [22]. Thus, low energy holes contained in the systems might be scattered at the grain boundaries, which could improve the Seebeck coefficient but decrease the electrical conductivity.

Fig. 6(c) and 6(d) reveals the temperature dependence of thermal conductivity and lattice thermal conductivity of all the samples. Thermal conductivity is measured in the temperature range 300~973 K. Generally, thermal conductivity ( $\kappa$ ) is the combination of the lattice thermal conductivity ( $\kappa_l$ ), and the thermal conductivity due to electronic contribution ( $\kappa_e$ ). On doping, both the thermal conductivity and lattice thermal conductivity are found to be decreased for all the samples with increasing temperature. This decreasing of thermal conductivity might be a combination of phonon scattering, substitutional defects and second phase interaction. Phonon scattering

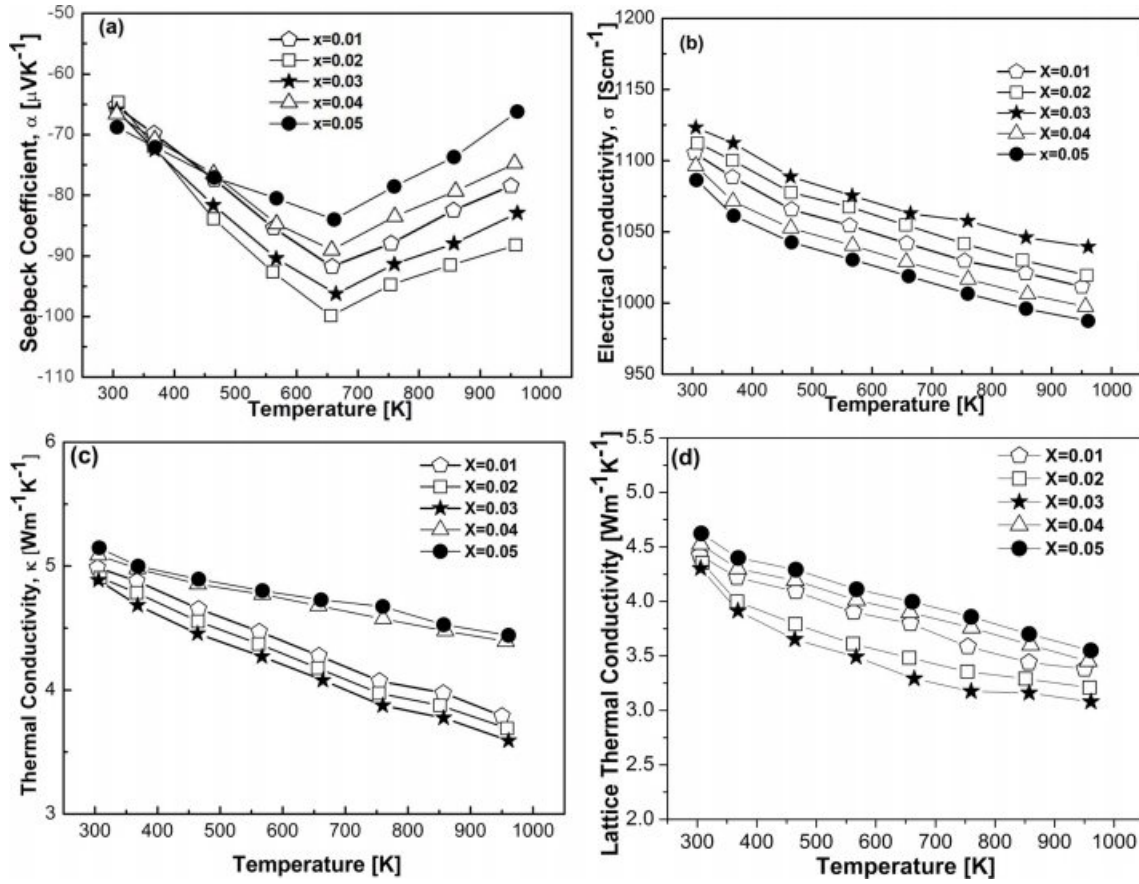


**Fig. 6.** Thermoelectric properties as a function of temperature and doping elements; (a) Seebeck coefficient, (b) electrical conductivity, (c) thermal conductivity, and (d) lattice thermal conductivity.

could be enhanced by increasing effective mass of the carriers [23]. Doping might introduce substitutional defects, which could disrupt the surrounding crystal structure and cause a local increase in the lattice strain energy [24]. Consequently, this atmosphere might decrease thermal conductivity over a considerable amount of substitutional defects. The second phases might also suppress grain growth by pinning effect during hot consolidation process and hence maintain high grain boundary density [25, 26]. Thermal conductivity due to electronic contribution is calculated by Wiedemann-Franz law using the formula  $\kappa_e = L\sigma T$ , where  $L$  is the Lorenz number ( $2 \times 10^{-8} \text{ W}\Omega\text{K}^{-2}$ ). It was found that the contribution of  $\kappa_e$  is very low compared to lattice

thermal conductivity. No incorporation of foreign elements was observed on thermal conductivity, which could be confirmed by EDS analysis given in Table 1.

ZT was calculated and displayed in Fig. 7. The maximum ZT of 0.21 was obtained for  $Fe_{0.97}Mn_{0.03}VSb$  at 567 K. Though a considerable improvement in ZT has achieved for n-type  $Fe_{1-x}Mn_xVSb$  HH alloys

**Table 1.** Measured EDS composition of the VHPed  $Fe_{1-x}Mn_xVSb$  HH samples.

Elements	Wt.%	At.%
Sb	45.14	41.93
V	27.45	25.72
Fe	25.01	28.66
Mn	2.40	3.69
Total	100.00	100.00

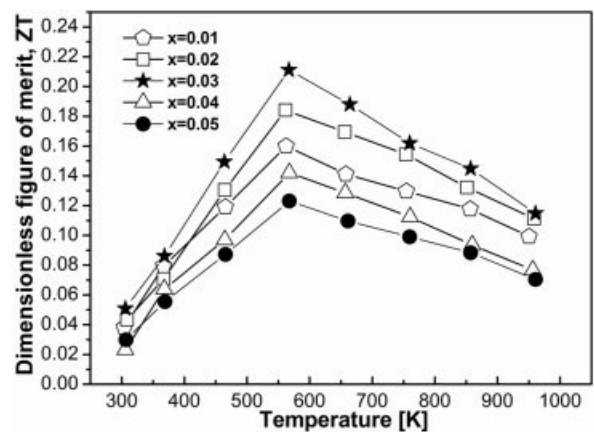


**Fig. 7.** Calculated ZT as a function of doping elements and temperature.

**Table 2.** Hall measured data for VHPed Fe<sub>1-x</sub>Mn<sub>x</sub>VSb HH alloys at room temperature.

Nominal composition	Hall coeff. (cm <sup>3</sup> /C)	Hall Mobility (cm <sup>2</sup> /Vsec)	Carrier conc. (10 <sup>20</sup> cm <sup>-3</sup> )
x=0.01	-0.381	431.66	7.39
x=0.02	-0.461	489.37	6.95
x=0.03	-0.406	512.73	5.21
x=0.04	-0.413	453.23	6.32
x=0.05	-0.433	481.68	6.16

compared to analogs, there remains much room for further improvement. This ZT is mainly due to the lower lattice thermal conductivity of the material systems and for relatively higher Seebeck coefficient. It might be expected that controlling the doping concentration and selecting the appropriate dopant could produce higher ZT than this experiment. One more possible way to enhance ZT might be multi-doping in different lattice sites which could reduce the thermal conductivity to a greater fraction and it might enhance ZT significantly [27].

### Conclusion

In summary, it can be said that n-type Fe<sub>1-x</sub>Mn<sub>x</sub>VSb (0.01 ≤ x ≤ 0.5) HH alloys were synthesized by employing MA process and subsequent VHP. All the samples were studied in the temperature range 300~973 K. Mn was chosen as an effective dopant for Fe because of similar size and nearly identical chemical properties. The considerable improvement was obtained for the sample Fe<sub>0.97</sub>Mn<sub>0.03</sub>VSb, which showed the peak ZT value of 0.21. This enhancement of ZT value is based on the considerable reduction of the thermal conductivity and comprehensive increase of the Seebeck coefficient. The Seebeck coefficient is increased considerably, possibly due to the optimized carrier concentration and enhanced effective mass of the carriers. Thermal conductivity was found to be decreased with increasing doping concentration and the lowest figure was found for x = 0.03. This lowest value of thermal conductivity is possibly due to second phase interaction and phonon scattering enhanced by increasing effective mass of carriers. Electrical conductivity was decreased with increasing temperature and the optimized value is found for Fe<sub>0.97</sub>Mn<sub>0.03</sub>VSb. The ZT obtained in this experiment is considered to be moderate but an effective TE device requires ZT ≥ 1.0. There are a lot of room for further improvement in ZT through reduction of thermal conductivity and enhancement of the Seebeck coefficient via optimization of appropriate doping at the other lattice sites.

### Acknowledgments

This work was supported by the Regional Innovation Center (RIC) Program, which was conducted by the Ministry of SMEs and Startups of the Korean Government.

### References

1. J. B. Neaton, *Nat. Nanotechnol.* 9 (2014), 876.
2. G. J. Snyder, E. S. Toberer, *Nat. Mater.* 7 (2008), 105.
3. Y. Z. Pei, X. Y. Shi, A. Lalonde, H. Wang, L. D. Chen, G. J. Snyder, *Nature*. 473 (2011), 66.
4. H. Hohl, A. P. Ramirez, C. Goldmann, G. Ernst, B. Wolfing, E. Bucher, *J. Phys. Condens. Matter* 11 (1999), 1697.
5. Y. Xia, V. Ponnambalam, S. Bhattacharya, A. L. Pope, S. J. Poon, T. M. Tritt, *J. Phys. Condens. Matter*. 13 (2001), 77.
6. R. Akram, Q. Zhang, D. Yang, Y. Zheng, Y. Yan, X. Su, X. Tang, *J. Electron. Mater.* 44 (2015), 3563.
7. D. P. Young, P. Khalifah, R. J. Cava, A. P. Ramirez, *J. Appl. Phys.* 87 (2000), 317.
8. M. Zou, J. F. Li, T. Kita, *J. of Sol. Stat. Chem.* 198 (2013), 125.
9. C. Uher, J. Yang, S. Hu, D. T. Morelli, G. P. Meisner, *Transport Properties of Pure and Doped MNiSn (M = Zr, Hf)*, *Phys. Rev. B.* 59 (1999), 8615.
10. Y. Xia, S. Bhattacharya, V. Ponnambalam, A. L. Pope, S. J. Poon, T. M. Tritt, *J. Appl. Phys.* 88 (2000), 1952.
11. S. Sakurada, N. Shutoh, *Appl. Phys. Lett.* 86 (2005), 082105 (1-3).
12. S. Populoh, M. Aguirre, O. Brunko, K. Galazka, Y. Lu, A. Weidenkaff, *Materials*, 6 (2013), 1326.
13. M. Schwall, B. Balke, *Phys. Chem. Chem. Phys.* 15 (2013), 1868.
14. X. Yan, W. Liu, H. Wang, S. Chen, J. Shiomi, K. Esfarjani, H. Wang, D. Wang, G. Chen, *Z. Ren, Energy Environ. Sci.*, 5 (2012), 7543.
15. E. Rausch, B. Balke, S. Ouardi, C. Felser, *Phys. Chem. Chem. Phys.* 16 (2014), 25258.
16. R. Stern, B. Dongre, G. K. H. Madsen, *Nanotechnology*, 27 (2016), 334002 (1-6).
17. S. -C. Ur, H. Choo, D. B. Lee, P. Nash, *Met. and Mate. Int.* 6 (2000), 435.
18. S. -H. Chang, C. -L. Li, K. -T. Huang, *Materials Transactions.* 58 (2017), 1190.
19. A. R. Denton, N. W. Ashcroft, *Vegard's Law*, *Phys. Rev. A.* 43 (1991), 3161.
20. J. Tobola, L. Jodin, P. Pecher, H. Scherrer, G. Venturini, B. Malaman, S. Kaprzyk, *Phys. Rev. B.* 64 (2001), 155103.
21. C. M. Bhandari, *CRC Handbook of Thermoelectrics (Boca Raton: CRC Press, 1995) p.68.*
22. J. P. Heremans, C. M. Thrush, D. T. Morelli, *Phys. Rev. B.* 70 (2004), 115334.
23. J. Cui, G. Cai, *W. RenRSC Adv.* 8 (2018), 21637.
24. Adrian P. Mouritz, *Introduction to Aerospace Materials (Chapter-4:Strengthening of metal alloys)*, Woodhead Publishing Limited (Sawston, England), 2012.
25. T. T. Khan, I. Mahmud, S. -C. Ur, *Kor. J. of Mat. Res.* 27 (2017), 416.
26. R. F. Decker, *Metallurgical Transactions.* 4 (1973), 2495.
27. P. Jozwik, Z. Bojar, *J. of Metallurgy and Materials.* 52 (2007), 321.